Article (refereed) - postprint

King, Stephen M.; Jarvie, Helen P.. 2012 Exploring how organic matter controls structural transformations in natural aquatic nanocolloidal dispersions. *Environmental Science & Technology*, 46 (13). 6959-6967. 10.1021/es2034087

Exploring How Organic Matter Controls Structural Transformations In Natural Aquatic Nanocolloidal Dispersions

Stephen M. King[*,‡] *and Helen P. Jarvie*[†]

ISIS Facility, STFC Rutherford Appleton Laboratory, Harwell Oxford, Didcot, OX11 0QX, UK

Centre for Ecology & Hydrology, Maclean Building, Crowmarsh Gifford, Wallingford, OX10 8AB, UK

stephen.king@stfc.ac.uk

RECEIVED DATE: 28-Sep-2011 **REVISION RECEIVED:** 10-Jan-2012

TITLE RUNNING HEAD: Structural Transformations in Aquatic Nanocolloids.

CORRESPONDING AUTHOR FOOTNOTE: * Corresponding author phone: +44 1235 446437; email: stephen.king@stfc.ac.uk. Joint first authors. ‡ ISIS Facility. † Centre for Ecology & Hydrology.

ABSTRACT: The response of the dispersion nanostructure of surface river bed sediment to the controlled removal and re-addition of natural organic matter (NOM), in the absence and presence of background electrolyte, was examined using the technique of small-angle neutron scattering (SANS). Partial NOM removal induced aggregation of the mineral particles, but more extensive NOM removal restored colloidal stability. When peat humic acid (PHA) was added to a NOM-deficient sediment concentration-related structural transformations were observed: at 255 mg/l PHA aggregation of the nanocolloid was actually enhanced, but at 380 mg/l PHA disaggregation and colloidal stability were

promoted. The addition of 2 mM $CaCl_2$ induced mild aggregation in the native sediment but not in sediments with added PHA, suggesting that the native NOM and the PHA respond differently to changes in ionic strength. A first attempt at using SANS to directly characterize the thickness and coverage of an adsorbed PHA layer in a natural nanocolloid is also presented. The results are discussed in the context of a hierarchical aquatic colloidal nanostructure, and the implications for contemporary studies of the role of dissolved organic carbon (DOC) in sustaining the transport of colloidal iron in upland catchments.

KEYWORDS: Natural, Aquatic, Colloid, Dispersion, Nanoparticle, Humic, Neutron, SANS, Structure, NOM, PHA, DOC.

Introduction

The physico-chemical transformation of *naturally-occurring* nanoparticles in the environment is increasingly recognized as having a key role in the transport, biogeochemical cycling and bioavailability of pollutants in aquatic ecosystems (*1, 2*). The transformations include particle aggregation, disaggregation, and surface modification; processes which usually take place in the presence of natural organic matter (NOM), and that respond to changes in temperature, concentration, pH or ionic strength. One particularly important arena in which these transformations come to the fore is in the degradation of soils.

Soils are, from a colloidal perspective, ostensibly heterogeneous complexes of inorganic nanoparticles (clays, minerals) and metal oxides 'glued' together by polydisperse organic polyanions (humic and fulvic acids, humins). However, under the right conditions, these humic substances can promote disaggregation of the complexes and thereby release, or simply enhance the mobility of, clay platelets and natural oxide nanoparticles in surface waters.

Over the last 20 years, water quality monitoring studies have shown widespread, and, in some cases dramatic, increases in dissolved organic carbon (DOC) concentrations in upland catchments across Europe and North America (*3, 4, 5, 6*). These increases in DOC concentrations have been attributed to

factors related to climate change (such as increased organic matter decomposition rates as a result of warming and the drying and aeration of peaty soils; *4, 6, 7*) and changes in atmospheric deposition chemistry (particularly the effects of declining sulphur and marine-derived sea-salt deposition on increased soil DOC solubility; *8, 9*). However, a recent study (*10*) has now linked trends in increasing concentrations of 'dissolved iron' (defined as <0.45 μm fraction) in UK upland rivers and lakes with the rising DOC concentrations. Thermodynamic modeling suggests that these increasing freshwater iron concentrations may be colloidal Fe(III) linked to oxyhydroxides and iron-containing clays. This work suggests that increasing DOC concentrations may help to stabilize iron-rich nanoparticles, promoting higher concentrations of mobile iron in the water column. This is of concern, because it is the upland water bodies which are the principle sources of potable water in the UK, and on current trends the EU limit for iron in drinking water (0.2 mg/l) will be exceeded by the end of the current decade. This example is thus a salient reminder of how the environmental transformation of nanoparticles can have wider public health and economic consequences beyond its immediate scientific significance.

There are a great many studies, indeed too many to reference adequately, concerning the colloidal stability of clay or metal oxide/hydroxide nanoparticle dispersions in the presence and absence of humic substances (but see *11, 12* and references therein). In general most use mixtures meticulously prepared in the laboratory from a 'monodisperse' clay (usually bentonite, kaolinite or montmorillonite), or crystalline mineral such as goethite, and a 'standard' humic substance in order to impart some control on the experimental parameter space (*13, 14, 15, 16, 17, 18a, 20, 21, 22*). Often these mineral nanoparticles are supplied as an aqueous slurry, but some studies start with dried powder for convenience. However dispersing mineral nanoparticles adequately can be a difficult process. Studies using actual samples sourced from the natural environment are rare (*23a*). Most studies also focus on the ability of the humic substances to confer colloidal *instability*, that is, to bring about aggregation. Rather fewer actively pursue disaggregation (*18b, 19a, 19b, 24*).

Many complementary investigative techniques have been deployed including sedimentation (*17*), rheology (*18b, 19a)*, electrokinetics (*18b, 19a*), imaging (*16, 25, 26, 27, 28*), and various forms of light scattering (*20*), particularly photon correlation spectroscopy (*13, 15, 29*). One unintentional consequence of the use of optical techniques (and indeed sedimentation and some atomic force microscopy) is that the length scales (ie, particle sizes) probed are typically hundreds to thousands of nm. Probing the structure of 'nanocolloids', defined as the <0.2 μm size regime, *particularly in the dispersion state*, is more challenging and where techniques such as low-angle scattering (diffraction) using X-rays (*14, 30*) or neutrons (*23a*), which utilize much shorter wavelengths than light, can be advantageous.

The importance of nanocolloids in this context is two-fold; first, they are more likely to represent the early stages of aggregate formation (or the latter stages of disaggregation) and, second, as we have come to appreciate in studies of engineered nanoparticles, physical and chemical properties at the nanoscale can be rather different to those of bulk matter.

In this paper, we explore the role of dissolved NOM on the nanostructure and aggregation/disaggregation behavior of natural aquatic colloidal material (stream bed sediments) by first the removal of NOM, and then the subsequent addition of peat humic acid (PHA). We also explore the impact of electrolyte on this behavior. To do this we exploit the unique capabilities of small-angle neutron scattering (SANS) as a means to probe the fractal structure of the nanocolloids (*23a*), and to selectively characterize the mineral and organic phases in the highly-turbid aqueous dispersions as they respond to the changing conditions.

Our observations suggest that the rising DOC concentrations observed in upland river water may not in themselves be sufficient to impart large-scale colloidal stability to iron oxhydroxides and iron-rich clays, but may instead be linked to elevated DOC levels in soil porewaters.

Experimental Section

Sediments. Fine surface river bed sediment was collected by vacuum sampling from a rural lowland agricultural river at Priors Farm (UK NGR ST89202843) in the Hampshire Avon catchment as previously described (*23b*). The chemical composition of this particular material is 6 % Fe(III). After collection, the wet sediment was stored in the dark at 5 - 8 °C to minimize latent biological activity. Different portions of the sediment were then subjected to a range of treatments: (i) to explore whether drying the sediment had any consequences for its subsequent redispersal, sediment was: (a) freeze-dried or (b) oven-dried in air at 110 °C; (ii) to investigate the role of NOM, sediment was treated with 30% $^{w}/_{w}$ hydrogen peroxide (H_2O_2, Sigma-Aldrich) at room temperature as a means to digest organic matter. Two different H_2O_2 treatments were applied: (a) *short-term*, where the sediment was subjected to one addition of H_2O_2 and then left for 48 hours before further use (as in our earlier work) and, (b) *long-term*, where multiple additions of H_2O_2 were made over the course of about 1 week until no further reaction was evident. This long-term H_2O_2-treated sediment was then left for a further 2 weeks before use except for daily additions of small amounts of deionised water (H_2O, >10MΩ resistivity, SG euRO) to prevent the sediment slurry drying out. The different H_2O_2 treatments were intended to result in different degrees of NOM removal. The effect of the H_2O_2 treatment process on the sediment is evident in Figure 1.

Peat humic acid. Purified PHA was prepared from a commercial Irish horticultural peat following the standard IHSS procedure (*31*) and extensively characterized (*32*). It had an elemental composition 52.1% C : 5.1% H : 42.8% other, a molecular weight at the lower end of the scale for humic acids (M_w 23 kDa in 1 M NaCl), and lower ash and residual metal levels than are found in many other available commercial or research samples.

Sample preparation. For the SANS experiment, each of the different treated sediments were variously redispersed, without filtration, into deionised water, heavy water (D_2O, 99.9 atom% D, Sigma-Aldrich or Fluorochem Ltd), H_2O/D_2O mixtures, or 2 mM calcium chloride solution ($CaCl_2$, to model the background ionic strength of river water). Sediment concentrations were adjusted to be approximately 5% $^{w}/_{w}$ before the experiment (*circa* 1.8% $^{v}/_{v}$) but the *actual* concentrations of all

samples were determined gravimetrically *post*-experiments and it is these latter values that have been used in the data analysis. Several of these different sediment samples were prepared in replicate to help assess natural sample variability.

PHA was added to samples of the short-term H_2O_2-treated sediment in the different media at *initial* concentrations of 255 mg PHA/l and 380 mg PHA/l and the pH adjusted to pH 5.8±0.1 by the addition of 0.1M sodium hydroxide solution (NaOH, Sigma-Aldrich). For samples in D_2O, pH = pD - 0.4, based on the pK for dissociation of deuterium ions. The PHA concentrations above were calculated to correspond to points early and late on in the 'plateau' region of a typical PHA adsorption isotherm (see **Supporting Information**). Whilst such a calculation will never be exact, these concentrations are within the range of DOC concentrations found in peat soil porewater (*33*) if it is assumed that all the carbon in the PHA is dissolved. The corresponding *equilibrium* PHA concentrations in our samples are estimated to be 22 mg PHA/l and 40 mg PHA/l, respectively.

Small-angle neutron scattering. SANS data were collected on the neutron diffractometer LOQ (*34*) at the ISIS Spallation Neutron Source, Didcot, UK and analyzed as previously described (*23b*). The reader unfamiliar with the principles and practice of SANS is encouraged to consult this reference. The sediment samples were placed in 2 mm path length quartz cuvettes (Hellma GmbH, Type 120-QS, volume 500 µl), briefly sonicated, then mounted on a special computer-controlled sample changer able to slowly rotate the cuvettes about the axis of the neutron beam. This prevented sedimentation of the larger colloidal material present. The measurements were performed at ambient temperature (24.5±2.0 °C). Data collection times varied between 30 min and 3 hours per sample. All data were corrected for neutron absorbtion by the sample (*cf* Beer-Lambert law), background scattering from the instrument, cuvettes and dispersion media, and placed on an absolute intensity scale. The neutron scattering length density of the sediment was experimentally re-determined from its scattering in a range of H_2O : D_2O mixtures to be $+4.01\times10^{10}$ cm^{-2}, in good agreement with our earlier work. This value corresponds to a mixture 34% H_2O. In such a mixture the mineral component of the sediment becomes

almost invisible to the neutrons (*cf* refractive index matching) and is said to be at 'contrast match'. In pure H_2O dispersions the mineral scattering is maximized, whilst in D_2O-rich dispersions the scattering from the organic component is maximized. These conditions are termed 'off-match'. This 'contrast variation' principle is one of the key benefits of using SANS. Analytical scattering laws were least-squares fitted to the various SANS datasets in order to extract a range of parameters characterizing the samples. As before, these scattering laws fell into two classes: those that described physically-plausible (but nonetheless assumed) dispersions of fractal clusters of *spherical* particles, and those that described mathematically-consistent (but nonetheless phenomenological) density variations with characteristic length scales. The former were more successful at modelling the data. Scattering laws for (even quite polydisperse) discrete *regular* objects (ie, spheres, ellipsoids, platelets, etc) were, however, substantially inferior. Representative SANS data and details about its analysis may be found in the **Supporting Information**.

Results and Discussion

Structural transformations in the native sediment induced during sediment preparation. The first question to be addressed was whether drying the sediment, and then redispersing it, actually had consequences for the structure of the nanocolloids present. Whilst preparing samples of aquatic nanocolloids for study from natural sediment *dispersions* obviously ought be the 'gold standard', it nevertheless adds an additional layer of complexity over using a dry powder as discussed in the Experimental Section.

Table 1 shows the results from SANS measurements on four different sets of sediment samples, each prepared in replicate. It is quite clear that the samples in which the sediment was dried and then redispersed in H_2O (samples E1.3 through E1.6) exhibit greater variability in cluster correlation lengths ('size'; ψ), cluster aggregation number (N_{agg}), and mass fractal dimension (D_m) than the samples made with sediment which was kept wet throughout (samples E1.1 and E1.2). In fact the similarity of the parameters for the latter two samples are impressive; these were not one batch of material divided

between two cuvettes, but two separate sample preparations. Overall the length scales and fractal dimensions measured are consistent with our earlier work (*23a*). The values of D_m emphasize that the underlying structure of all the nanocolloids studied is mass fractal, as is typical of systems assembled from smaller sub-units. The values of the power law exponent n ($\propto D_m$) are also larger than those expected from structures arising as a result of diffusion-limited ($n_{DLCA} \approx 1.75$-1.80) or reaction-limited ($n_{RLCA} \approx 2.10$-2.25) cluster aggregation processes.

Of the dried sediment samples, those with larger values of N_{agg} and ψ (samples E1.4 and E1.6) had smaller values of D_m, approaching 2. This could suggest that the larger clusters had 'collapsed' to form more 'plate-like' structures on drying and is a reasonable expectation for clay minerals.

In summary, this first set of results indicate that drying sediment makes it much more difficult to redisperse effectively in water, resulting in nanocolloids which are more heterogeneous in organization than in the native dispersion. Therefore, all of the remaining samples for this work were prepared using sediment that had been kept wet.

Structural transformations in the native sediment induced by the addition of background electrolyte. The effects are subtle but, when sediment is dispersed in 2 mM $CaCl_2$ (samples E1.9 and E1.10), there are increases in D_m (from 2.47 in H_2O to 2.55 - 2.76), $R_{primary}$ (from 3.2 nm in H_2O to almost 4 nm), ψ (from 7.7 nm in H_2O to nearer 9 nm) and ξ (from around 36 nm in H_2O to over 38 nm), but a reduction in N_{agg} (from 10 - 11 in H_2O to 8). Taken together these results suggest that the electrolyte promotes the formation of slightly larger, but more compact, clusters through the aggregation of fewer, but larger, primary particles. Interestingly, these clusters are also *less* polydisperse in size (they have a larger τ). A possible mechanism for such aggregation, in the form of Ca^{2+}-mediated bridging between NOM-coated particles, has been reported recently (*18b*). However, in the present system the relatively high NOM content of the native sediment (18% loss on ignition, *23a*) means that the primary

mode of dispersion stabilization is more likely to be steric than electrostatic. It is thus perhaps not surprising if the effect of the electrolyte is small.

Structural transformations in the native sediment induced by NOM removal. Table 2 compares the results from SANS measurements on H_2O_2-treated sediment (two replicate samples E1.7 and E1.8, and sample E1.11) with the native wet sediment (sample E1.1). Focusing first on samples E1.7 and E1.8, those in which only *partial* NOM removal was expected, several significant differences in the structure of the nanocolloids are evident: there is a 5- to 10-fold increase in $R_{primary}$ (from 3 nm for the native sediment to 15 – 34 nm), a 3- to 5-fold increase in ψ (from 8 nm for the native sediment to 22 - 42 nm), a 3- to 4-fold reduction in N_{agg} (from 10 – 11 for the native sediment to just 2 – 3), and a reduction in D_m from 2.47 for the native sediment to 2.08 - 2.19. These results suggest that partial oxidation of the NOM has resulted in substantial particle aggregation, perhaps leading to large, plate-like, clusters.

In stark contrast to the above, as illustrated by sample E1.11, *substantial* NOM removal appears to result in disaggregation of particles, leading to *clusters* whose structure is remarkably similar to those found in the native sediment (even though the overall structure of the dispersion is different, as indicated by the even higher value of D_m).

We postulate that, in the native sediment, the relatively high NOM content results in what is effectively steric stabilization of the dispersion. Short-term peroxide treatment removes the more labile organic component, but leaves a refractory organic component to promote bridging between clay particles and thus aggregation. Removal of this residual organic material by longer-term H_2O_2-treatment removes this bridging mechanism and, as electrostatic forces come into play, re-stabilizes the dispersion.

Structural transformations in NOM-deficient sediment induced by the addition of PHA. The effects of adding PHA to sediment subjected to partial NOM removal is also compared in Table 2. Addition of 255mg/l PHA in H_2O (sample E3.1) did not significantly change the structure of the

nanocolloid (*cf* samples E1.7 and E1.8), except for a small reduction in D_m (from 2.08 – 2.19 in the absence of PHA to 2.01 in the presence of PHA) indicative of even more plate-like structure. These observations can be rationalized as the PHA further strengthening *existing* interparticle bridging within the clusters as would be consistent with PHA adsorbing at low surface coverage (*35*).

In contrast, addition of 380 mg/l PHA in H2O (sample E3.2) resulted in a dramatic reduction in $R_{primary}$ (from 15 – 34 nm in the absence of PHA or 18 nm at 255 mg/l PHA to 8 nm) and ψ (from 22 – 42 nm in the absence of PHA or 31 nm at 255mg/l PHA to 13 nm), and an increase in D_m (from about 2.1 in the absence of PHA or 2.01 at 255 mg/l PHA to 2.25). These results suggest that the higher PHA concentration improves the stability of the dispersion, most likely through steric repulsion. This would be consistent with PHA adsorbing at higher surface coverage.

When the PHA additions are repeated in 2 mM $CaCl_2$ solution instead of H_2O (samples E3.3 and E3.4), the same trends are observed but the changes are even more marked. In fact the structural parameters for sample E3.4 (treated sediment plus 380 mg/l PHA, at pH6, in 2mM $CaCl_2$) bear a remarkable resemblance to those for the native sediment (sample E1.1).

These results suggest that H_2O_2-treated samples to which PHA has been added undergo dispersion/disaggregation in the presence of electrolyte. This is actually the reverse effect to that observed for a native sediment sample, discussed above, where addition of electrolyte induced mild aggregation and illustrates that the way in which the PHA interacts with the mineral particles in the presence of electrolyte differs to that of the native NOM. Similar observations have been made previously (*17*). The explanation for this difference in behavior is likely a combination of several factors: a weakening of the Ca^{2+} bridging mechanism, a less favorable ratio of organic matter to calcium loading (*18b*), and the fact that the native NOM contains a mixture of both humic *and* fulvic acids (FA). Indeed, comparisons of the adsorbtion of HA and FA onto goethite show that HA adsorbtion is stronger and more pH- and ionic strength- dependent (*21, 22*).

With the treated sediments dispersed in H_2O the mineral component and the organic component both contribute to the observed scattering, but the scattering from the mineral component is approximately 3 to 5 times stronger (see the **Supporting Information)**. In D_2O these contrast conditions are inverted. Thus, comparing the structural parameters for sample E3.6 in Table 2 (in D_2O) with those from sample E3.2 (the analogous sample in H_2O) gives a complementary perspective of the same dispersion. The structural parameters are broadly comparable, though the 'organic-centric' data from sample E3.6 suggests the presence of somewhat smaller clusters of higher fractal dimension. This may, for example, be related to differences in the degree of dissociation of the ionisable groups on the PHA in D_2O.

What happens to the native NOM during the structural transformations? This was assessed by preparing an analogous range of samples in which the mineral component of the sediment was contrast matched to the dispersion medium, meaning that the observed scattering was primarily contributed by the organic component (plus a residual signal from mineral components differing in neutron scattering length density from the average). The results are summarized in Table 3.

Comparing first just the native wet sediment at contrast match (sample E2.11) with the same sediment only dispersed in H_2O (sample E1.1), it is seen that there is a reduction in $R_{primary}$ (from 3 in H_2O to 1), ψ (from 8 in H_2O to 3), N_{agg} (from 11 in H_2O to 6), and n (from 3.30 in H_2O to 2.81), but an increase in D_m (from 2.47 in H_2O to 2.66). Although not shown in the table, results from fitting the contrast match data to the dual-length scale 2-phase model (*23b*) also showed a significant reduction in the short correlation length ζ (from 10 nm in H_2O to 7 nm), but a less marked change in the long correlation length ξ (reducing from 36 nm in H_2O to 34 nm). The clear message from these analyses is that suppressing the scattering from the mineral fraction to highlight the organic component moves the focus to shorter length scales. The change in n is itself indicative of a change in the structural hierarchy responsible for the scattering; away from something more particulate with a rough (or fractal) surface to something more like a loose network (*23b*). This provides an insight into how the organic fraction mediates the overall structure of the clusters: changes at longer length scales are themselves a

consequence of underlying changes on shorter length scales. In other words, natural aquatic nanocolloids have a hierarchical structure. This conclusion supports existing interpretations (*2, 12, 23a, 36*). It may also help to explain the structural parameters from samples E3.6 and E3.2 in the previous sub-section, where smaller clusters of higher fractal dimension were observed when the focus was on the organic component, but larger clusters of lower fractal dimension were observed when the contrast conditions favored the mineral component. A possible picture therefore is one of clusters of organic material within, and associated with, clusters of mineral particles such that the overall structure of the nanocolloid is determined by the extent and strength of adsorbtion of the organic matter. The scattering law we use to interpret these systems, however, only assumes a single population of clusters.

A comparison of the parameter values for the contrast-matched native sediment in the absence (sample E2.11) and presence (sample E2.12) of 2mM $CaCl_2$ suggests that the underlying structure of the native NOM itself is not particularly sensitive to changes in ionic strength of this magnitude. Whereas the same comparison 'off-match' (*ie* in H_2O, samples E1.1, E1.9 & E1.10 in Table 1, discussed earlier) hinted at particle aggregation. This difference could be explained if the principle impact of the electrolyte on the native sediment were to alter the strength of the mineral-NOM interaction, rather than to alter the size and arrangement of the NOM *per se*.

Comparing samples E2.14 and E2.11, to investigate what happens to the refractory NOM remaining after short-term H_2O_2-treatment but under contrast match conditions, it is observed that there are small increases in $R_{primary}$ (from 1 nm in the native sediment to 3 nm), ψ (from 3 nm in the native sediment to 7 nm) and N_{agg} (from 6 in the native sediment to 9). The increases in $R_{primary}$ and ψ are both far smaller than were observed 'off-match' (samples E1.1, E1.7 and E1.8 in Table 2). In the 'off-match' data there is also a significant reduction in D_m. This is not observed at contrast match; the residual NOM maintains its general structure but seems to have associated somewhat. This would, of course, be consistent with greater aggregation of the nanocolloid as a whole, the conclusion drawn from the 'off-match' data.

What happens to the added PHA during the structural transformations? The effect of adding PHA to the short-term H_2O_2-treated sediment at contrast match may be seen by comparing the parameter values for samples E3.7 and E3.8 with those for sample E2.14. At a concentration of 255 mg/l PHA there are very large increases in $R_{primary}$ (from 3 nm in the absence of PHA to 57 nm) and ψ (from 7 nm in the absence of PHA to 112 nm), coupled with a significant decrease in D_m (from 2.71 in the absence of PHA to 1.94). There is also a small decrease in N_{agg}. Although not shown in the table, results from fitting these data to the 2-phase and dual-length scale 2-phase models (*23b*) also showed increases in the correlation lengths. Except for the behavior of D_m these observations differ from those found 'off-match', where the mineral component lost some dimensionality but length scales remained more or less unchanged. However, adding 380 mg/l PHA mimics the effect on the structure of the nanocolloid seen in the 'off-match' data; $R_{primary}$, ψ, N_{agg} and D_m all return to values more reminiscent of those seen in the native sample (and correlation lengths extracted from the 2-phase and dual-length scale 2-phase models were also reduced). The 380 mg/l data at contrast match, and indeed the 380 mg/l data in D_2O (sample E3.6 in the previous sub-section), therefore also seem to support the assertion that this concentration of organic matter helps to restabilize the dispersion.

Whilst the hitherto unusually large values of $R_{primary}$ and ψ extracted from the 255 mg/l PHA data at contrast match could be evidence of a rogue sample, the 380 mg/l PHA data, the fact that the values of D_m at 255 mg/l PHA both at contrast match and 'off-match' are so similar, and the consistency of all the other data we have presented, suggest that our sample preparation procedures are as robust as could be expected and that the 255 mg/l PHA data at contrast match require an explanation; indeed, sample E3.7 has the lowest value of D_m we have measured.

The conclusion drawn from the 'off-match' data was that adding a low concentration of PHA to the H_2O_2-treated sediment enhanced interparticle bridging in an already collapsed structure (induced by partial NOM removal). If that collapse also results in a change from a three-dimensional network-like structure to a more two-dimensional network structure then any organic matter between the particles will

lose conformational freedom. Length scales will diminish in some directions but lengthen in others. This can be easily visualized in the following way: first suppose that the organic component (whether it is NOM or PHA) is 'unconstrained' and free to explore the volume of a sphere of some radius (or radius-of-gyration) R. If that same organic matter is now 'constrained' by confining it inside a rectangular cuboid (*ie* the phase space is now less three-dimensional and more two-dimensional) of height and width R, the length of that cuboid will need to increase by a factor of $(4\pi/3)$ to maintain the same excluded volume. If the height or width of the cuboid diminishes below R the length of the cuboid must extend further. This is a simplistic argument, which ignores the possibility of the NOM or PHA aggregating or the excluded volume constraints changing, but does illustrate how the linear dimensions of 'deformable' objects can change quite markedly when the fractal dimension of their phase space changes. An alternative explanation, which maintains conformational freedom, is that the smaller fractal dimensions result from more 'open' clusters having a less compact spatial mass distribution. Therefore, since $mass(\psi) \propto \psi^{Dm}$ length scales would need to increase to compensate.

Characterizing the structure of adsorbed PHA layers. To a first approximation, at contrast match for the mineral component, the contribution to the scattering from just the *adsorbed* organic matter in a sediment sample can be extracted by subtracting the contributions from residual mineral scattering and any *unadsorbed* organic matter in the dispersion medium. The latter can in turn be approximated as a proportion of the scattering from just PHA solubilised in the same contrast match mixture (Sample B9 in Figure SI-3), where the proportion to subtract is determined by the equilibrium PHA concentration in a given dispersion. As discussed above, in sediment samples containing 380 mg/l PHA, C_{eq} is calculated to be about 40 mg/l; *ie*, approximately 10%. The scattering signal that remains can then be interpreted by application of a 'surface-Guinier' model (*37*). This model is outlined in the **Supporting Information**, but Figure 2 shows an example data set and model fit. For the short-term H_2O_2-treated sediment sample containing 380 mg/l added PHA the model estimates that the centre-of-mass of the adsorbed PHA layer, σ_{layer}, extends on average some 6.6 nm from the particle surfaces, and that the average amount of PHA adsorbed, Γ_{layer}, ranges from 1.8 – 5.7 mg/m^2 for values of $R_{primary}$ of 4 nm and

40 nm, respectively. These values of σ_{layer} and Γ_{layer} assume a bulk density for the PHA of 1.5 g/cm^3 (*38*). Broadly similar numbers can be obtained from the 255 mg/l PHA dataset but the model fit has a much poorer χ^2 measure. These are all very reasonable values in terms of how they compare with those in the 'soft matter' literature (*35*), where this type of analysis was born, but the more pertinent question is how they sit in the context of this work. Fortunately the value of σ_{layer} also seems quite reasonable when compared to the values of ζ, ξ and ψ we have determined, especially if one considers that any 'polymeric' organic matter may extend several times σ_{layer} (density distributions for physically adsorbed polymers are often 'exponential-like'). It also fits quite nicely with recent thermodynamic models of mineral-humic adsorbtion (*22*), and with the shorter characteristic length scales for the structural hierarchy reported in our earlier work (*23a*).

When one considers that the specific surface area of the mineral particles is likely to be several tens of m^2 per g the estimates for Γ_{layer} probably represent 100 – 300 mg/g. Whilst this is a rather greater degree of adsorption than our earlier calculation proposed, it is nevertheless still well within the range of reported values for a variety of mineral-humic systems (*18a, 21, 39, 40, 41*). And, as we point out in the **Supporting Information**, our adsorbtion calculation was based on a rather conservative isotherm. With a better optimized system, and much higher quality data, as will be possible on the emerging next-generation SANS instruments, this type of approach may in the future offer new insights into our understanding of natural aquatic nanocolloids.

Relevance to structural transformations in the natural environment. We have shown that organic matter is a very important control on stability and structural transformations in natural aquatic nanocolloid dispersions. Partial removal of the NOM from organically-enriched stream sediments promotes strong aggregation, as the remaining refractory organic matter bridges between mineral nanoparticles, but this behavior can be readily reversed by adding back organic matter (such as PHA) at concentrations resulting in adsorption at high surface coverage. Sediments in which more rigorous removal of the NOM has taken place remain dispersed, no doubt stabilized by electrostatic forces. The

effect of electrolyte (ionic strength) on the dispersion stability appears to depend on the actual nature of the organic matter present, and on its degree of adsorbtion. These factors all combine in a complex structural hierarchy that determines the overall structure of the nanocolloid. One consequence of this is that if a natural aquatic nanocolloid is allowed to dry out its native structure will be lost and may be difficult, if not impossible, to recover.

Based on its carbon content, the higher PHA concentration of 380 mg/l used in this work, and which was able to promote dispersion of the mineral nanoparticles, corresponds to a DOC concentration of 200 mg/l (assuming all the PHA was solubilised). This is at least an order of magnitude higher than typical *river* DOC concentrations (*4, 42*), but is much more typical of DOC concentrations occurring in soil porewater in peaty soils (*7, 33*). This in turn suggests that the rising DOC concentrations in river water may *per se* not be sufficient to impart large-scale colloidal stability to the clay particles and iron oxhydroxides. Instead, the observed colloidal stability, and rising dissolved iron concentrations, may be linked to elevated DOC levels in soil porewaters, resulting from higher levels of *in situ* sorption of humic substances to the mineral nanocolloids within the soil. When these nanocolloids are then flushed into the stream network, the high levels of adsorbed organic matter impart greater stability and dispersion during transport within the water column.

Acknowledgements

The peat humic acid was kindly prepared and characterized by Dr Chris Milne, and provided by Dr David Kinniburgh, of the British Geological Survey. Dr Elizabeth Palmer-Felgate of the Centre for Ecology & Hydrology assisted with collection of the sediment, and Linda Armstrong (CEH) assisted with the preparation of the samples. Neutron beam time (Experiment No. RB610166) was provided by the Council for the Central Laboratory of the Research Councils (CCLRC, now the Science & Technology Facilities Council). The photograph in Figure 1 was taken by Stephen Kill, CCLRC. The authors would also like to thank the two anonymous reviewers for their comments which helped to bring a new perspective to the results.

Supporting Information Available

Calculation of the PHA concentrations used, composition of the sediment, representative SANS data, details of the SANS scattering functions used to analyse the data, and the relevant SANS contrast factors. This material is available free of charge via the Internet at http://pubs.acs.org.

Literature Cited

(1) Buffle, J. The Key Role of Environmental Colloids/Nanoparticles for the Sustainability of Life. *Environ. Chem.* **2006**, *3*, 155-158.

(2) Lead, J. R.; Wilkinson, K. J. Aquatic Colloids and Nanoparticles: Current Knowledge and Future Trends. *Environ. Chem.* **2006**, *3*, 159-171.

(3) Driscoll, C. T.; Driscoll, K. M.; Roy, K. M.; Mitchell, M. J. Chemical response of lakes in the Adirondack Region of New York to declines in acidic deposition. *Environ. Sci. Tech.* **2003**, *37*, 2036-2042.

(4) Worrall, F.; Harriman, R.; Evans, C. D.; Watts, C. D.; Adamson, J.; Neal, C.; Tipping, E.; Burt, T.; Grieve, I.; Monteith, D.; Naden, P. S.; Nisbet, T.; Reynolds, B.; Stevens, P. Trends in dissolved organic carbon in UK rivers and lakes. *Biogeochem.* **2004**, *70*, 369-402.

(5) Skjelkvåle, B. L.; Stoddard, J.; Jeffries, D.; Torseth, K.; Hogasen, T.; Bowman, J.; Mannio, J.; Monteith, D. T.; Mosello, R.; Rogora, M.; Rzychon, D.; Vesely, J.; Wieting, J.; Wilander, A.; Worsztynowicz, A. Regional scale evidence for improvements in surface water chemistry 1990-2001. *Environ. Poll.* **2005**, *137*, 165-176.

(6) Evans, C. D.; Chapman, P. J.; Clark, J. M.; Monteith, D. T.; Cressers, M. S. Alternative explanations for rising dissolved organic carbon export from organic soils. *Glob. Change Biol.* **2006**, *12*, 2044-2053.

(7) Freeman, C.; Evans, C. D.; Monteith, D.T.; Reynolds, B.; Fenner, N. Export of organic carbon from peat soils. *Nature*. **2001**, *412*, 785.

(8) Krug, E. C.; Frink, C. R. Acid rain on acid soil: a new perspective. *Science*. **1983**, *211*, 520-525.

(9) Monteith, D. T.; Stoddard, J. L.; Evans, C. D.; de Wit, H. A.; Forsius, M.; Høgåsen, T.; Wilander, A.; Skjelkvåle, B. L.; Jeffreies, D. S.; Vuorenmaa, J.; Keller, B.; Kopácek, J.; Vesely, J. Dissolved organic carbon trends resulting from changes in atmospheric deposition chemistry. *Nature.* **2007**, *450*, 537-541.

(10) Neal, C.; Lofts, S.; Evans, C. D.; Reynolds, B.; Tipping, E.; Neal, M. Increasing Iron Concentrations in UK Upland Waters. *Aquat. Geochem.* **2008**, *14*, 263-288.

(11) Filella, M.; Buffle, J. Factors controlling the stability of submicron colloids in natural-waters. *Coll. Surf. A*. **1993**, *73*, 255-273.

(12) Buffle, J.; Wilkinson, K. J.; Stoll, S.; Filella, M.; Zhang, J. A Generalized Description of Aquatic Colloidal Interactions: The Three-colloidal Component Approach. *Environ. Sci. Tech.* **1998**, *32*, 2887-2899.

(13) Kretzschmar, R.; Holthoff, H.; Sticher, H. Influence of pH and Humic Acid on Coagulation Kinetics of Kaolinite: A Dynamical Light Scattering Study. *J. Coll. Int. Sci.* **1998**, *202*, 95-103.

(14) Tombácz, E.; Szekeres, M.; Baranyi, L.; Michéli, E. Surface modification of clay minerals by organic polyions. *Coll. Surf. A*. **1998**, *141*, 379-384.

(15) Tombácz, E.; Filipcsei, G.; Szekeres, M.; Gingl, Z. Particle aggregation in complex aquatic systems. *Coll. Surf. A*. **1999**, *151*, 233-244.

(16) Maurice, P. A.; Namjesnik-Dejanovic, K. Aggregate Stuructures of Sorbed Humic Substances Observed in Aqueous Solution. *Environ. Sci. Tech.* **1999**, *33*, 1538-1541.

(17) Jarvis, P.; Jefferson, B.; Parsons, S. A. How the Natural Organic Matter to Coagulant Ratio Impacts on Floc Structural Properties. *Environ. Sci. Tech.* **2005**, *39*, 8919-8924.

(18) Majzik, A.; Tombácz, E. Interaction between humic acid and montmorillonite in the presence of calcium ions. (a) I. Interfacial and aqueous phase equilibria: Adsorption and complexation. *Org. Geochem.* **2007**, *38*, 1319-1329. (b) II. Colloidal interactions: Charge state, dispersing and/or aggregation of particles in suspension. *Org. Geochem.* **2007**, *38*, 1330-1340.

(19) Harbour, P. J.; Dixon, D. R.; Scales, P. J. The role of natural organic matter in suspension stability. (a) 1. Electrokinetic-rheology relationships. *Coll. Surf. A.* **2007**, *295*, 38-48. (b) Modelling of particle-particle interaction. *Coll. Surf. A.* **2007**, *295*, 67-74.

(20) Bilanovic, D. D.; Kroeger, T. J.; Spigarelli, S. A. Behaviour of humic-bentonite aggregates in diluted suspensions. *Water SA*. **2007**, *33*, 111-116.

(21) Weng, L.; Van Riemsdijk, W. H.; Koopal, L. K.; Hiemstra, T. Adsorption of Humic Substances on Goethite: Comparison between Humic Acids and Fulvic Acids. *Environ. Sci. Tech.* **2006**, *40*, 7494-7500.

(22) Weng, L.; Van Riemsdijk, W. H.; Hiemstra, T. Adsorption of humic acids onto goethite: Effects of molar mass, pH and ionic strength. *J. Coll. Int. Sci.* **2007**, *314*, 107-118.

(23) Jarvie, H. P.; King, S. M. Small-Angle Neutron Scattering Study of Natural Aquatic Nanocolloids. (a) *Environ. Sci. Tech.* **2007**, *41*, 2868-2873. (b) Supplementary Information for same.

(24) Baalousha, M.; Aggregation and disaggregation of iron oxide nanoparticles: Influence of particle concentration, pH and natural organic matter. *Sci. Tot. Environ.* **2009**, *407*, 2093-2101.

(25) Leppard, G. G. Size, morphology and composition of particulates in aquatic ecosystems – Solving speciation problems by Correlative Electron-Microscopy. *Analyst.* **1992**, *117*, 595-603.

(26) Myneni, S. C. B.; Brown, J. T.; Martinez, G. A.; Meyer-Ilse, W. Imaging of Humic Substance Macromolecular Stuctures in Water and Soils. *Science.* **1999**, *286*, 1335-1337.

(27) Wilkinson, K. J.; Balnois, E.; Leppard, G. G.; Buffle, J. Characteristic features of the major components of freshwater colloidal organic matter revealed by transmission electron and atomic force microscopy. *Coll. Surf. A*. **1999**, *155*, 287-310.

(28) Assemi, S.; Hartley, P. G.; Scales, P. J.; Beckett, R. Investigation of adsorbed humic substances using atomic force microscopy. *Coll. Surf. A*. **2004**, *248*, 17-23.

(29) Ledin, A.; Karlsson, S.; Duker, A.; Allard, B. Applicability of Photon-Correlation Spectroscopy for measurement of concentration and size distribution of colloids in natural-waters. *Anal. Chim. Act.* **1993**, *281*, 421-428.

(30) Malekani, K.; Rice, J. A.; Lin, J. S. Comparison of techniques for determining the fractal dimension of clay minerals. *Clays Clay Min.* **1996**, *44*, 677-685.

(31) Thurman, E. M.; Malcolm, R. L. Preparative isolation of aquatic humic substances. *Environ. Sci. Tech.* **1981**, *15*, 463-466.

(32) Milne, C. J. Measurement and modeling of ion binding by humic substances. PhD thesis. University of Reading, UK. **2000**.

(33) Aguilar, L.; Thibodeaux, L. J. Kinetics of peat soil dissolved organic carbon release from bed sediment to water. Part 1. Laboratory simulation. *Chemosphere*. **2005**, *58*, 1309-1318.

(34) SANS instrument web page: http://www.isis.stfc.ac.uk/instruments/loq/ .

(35) Fleer, G. J.; Cohen Stuart, M. A.; Scheutjens, J. M. H. M.; Cosgrove, T.; Vincent, B. Polymers at Interfaces. Chapman & Hall. London. **1993**.

(36) Kretzschmar, R.; Borkovec, M.; Grolimund, D; Elimelech, M. Mobile subsurface colloids and their role in contaminant transport. *Adv. Agronomy*. **1999**, *66*, 121-193.

(37) King, S. M.; Griffiths, P. C.; Cosgrove, T. Using SANS to Study Adsorbed layers in Colloidal Dispersions. In *Applications of Neutron Scattering to Soft Condensed Matter*. Gabrys, B. J., Ed. Gordon & Breach. New York. 2000. Chapter 4.

(38) Dinar, E.; Mentel, T. F.; Rudich, Y. The density of humic acids and humic like substances (HULIS) from fresh and aged wood burning and pollution aerosol particles. *Atmos. Chem. Phys. Discuss.* **2006**, *6*, 7835-7867.

(39) Walker, H. W.; Bob, M. M. Stability of particle flocs upon addition of natural organic matter under quiescent conditions. *Wat. Res.* **2001**, *35*, 875-882.

(40) Tombácz, E.; Libor, Z.; Illés, E.; Majzik, A.; Klumpp, E. The role of reactive surface sites and complexation by humic acids in the interaction of clay mineral and iron oxide particles. *Org. Geochem.* **2004**, *35*, 257-267.

(41) Berka, M.; Palau Pla, S.; Rice, J. A. Characterization of Soil Particle Surfaces Using Adsorption Excess Isotherms. *Langmuir*. **2006**, *22*, 687-692.

(42) Worrall, F.; Burt, T. P. Trends in DOC concentration in Great Britain. *J. Hydrology.* **2007**, *346*, 81-92.

Figures

Figure 1. Some of the actual sediment samples measured. (L-R): E1.2, E1.3, E1.7 & E2.9. The sample codes are explained in the main text and tables except for Sample E2.9, which is an native sediment sample in a dispersion medium that is predominantly heavy water (D_2O). Note the slight variations in the concentration of the dispersed phases which must be allowed for in the SANS data analysis. Also note the lighter shade of E1.7, the only one of the four samples to have been subjected to treatment with hydrogen peroxide. To offset sedimentation during the SANS measurements the cuvettes were rotated about the axis of the neutron beam. For scale, the cuvette bodies are approximately 20 mm in diameter.

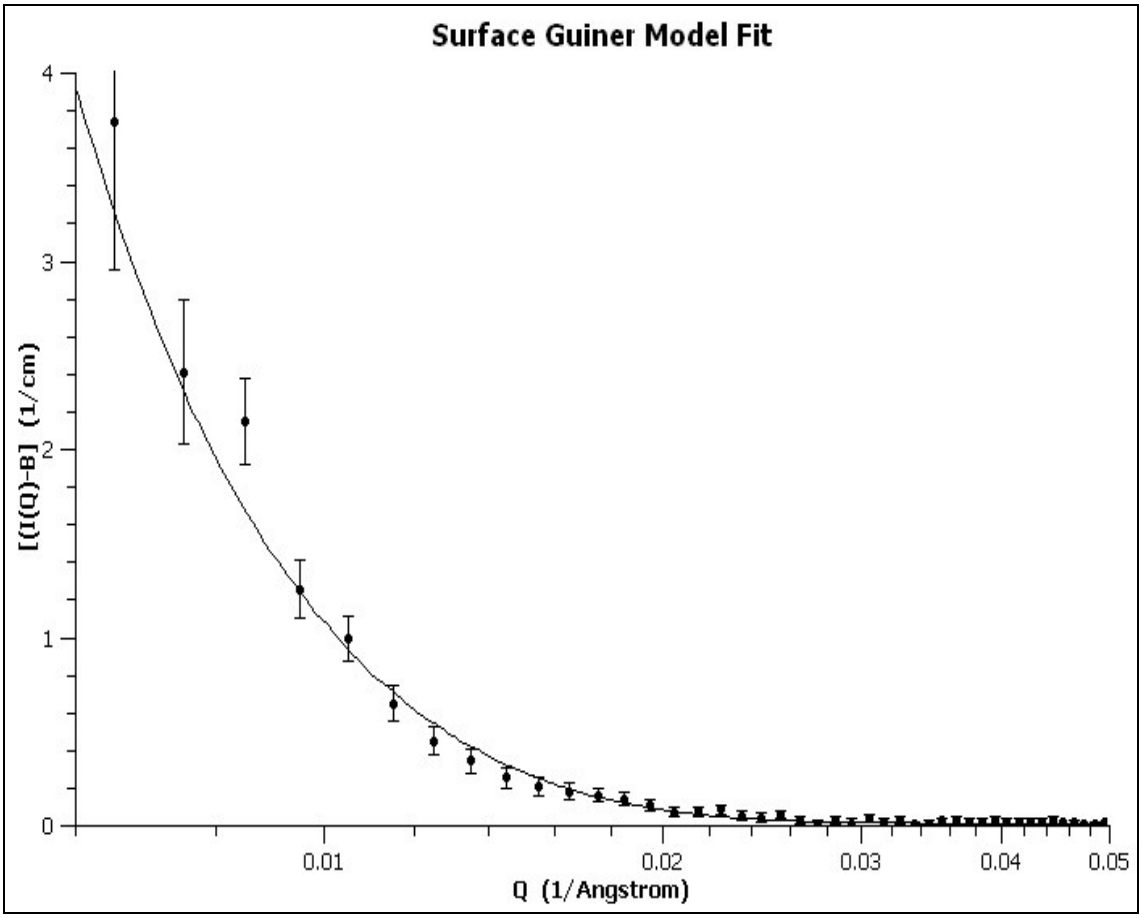

Figure 2. The scattering from only the surface adsorbed PHA in a short-term H_2O_2-treated sediment with 380 mg/l added PHA; *ie*, the subtraction Sample E3.8 *minus* Sample E2.14 *minus* 10% of Sample B9 (to allow for solubilised PHA at a C_{eq} of about 40 mg/l, see Figure SI-3), together with a 'surface Guinier' model fit to the data (Equation SI-12). The fit provides estimates of the thickness of the adsorbed layer and the amount of PHA adsorbed.

Tables

Table 1. Structural characteristics for the native sediment replicates before and after drying and in the presence of background electrolyte. Indicative errors on the fractal dimensions represent one standard deviation as derived from the model-fitting analysis.

Code	Sample & Matrix	ϕ [a]	n [b]	2-phase model [c]	Dual length 2-phase model [d]		Fractal Aggregates Model [e]				
		%		ζ (nm)	ζ (nm)	ξ (nm)	R_{pri} (nm)	N_{agg}	τ	D_m	ψ (nm)
	In H_2O:										
E1.1	Wet sediment (Replicate #1)	1.90	3.30	16.4	10.4	36.2	3.2	11	1.30	2.47 ± 0.02	7.8
E1.2	Wet sediment (Replicate #2)	1.65	3.27	15.8	11.4	36.5	3.3	10	1.31	2.47 ± 0.02	7.7
E1.3	Freeze-dried sediment (Replicate #1)	1.43	3.33	17.5	11.2	38.2	3.2	10	1.34	2.61 ± 0.02	7.5
E1.4	Freeze-dried sediment (Replicate #2)	1.42	3.30	17.1	10.2	36.6	2.9	33	1.30	2.23 ± 0.04	11.9
E1.5	Oven-dried sediment (Replicate #1)	1.36	3.32	17.9	11.5	38.1	3.9	8	1.46	2.74 ± 0.01	8.3
E1.6	Oven-dried sediment (Replicate #2)	1.37	3.35	18.1	12.1	40.5	3.6	29	1.31	2.24 ± 0.07	13.7
	In 2mM $CaCl_2$ / H_2O:										
E1.9	Wet sediment (Replicate #1)	1.88	3.20	15.1	10.1	38.4	3.9	8	1.43	2.55 ± 0.01	8.5
E1.10	Wet sediment (Replicate #2)	1.69	3.19	15.3	10.5	38.6	3.4	8	1.56	2.76 ± 0.01	7.6

[a] Assuming a mineral density of 2.75 g/cm^3 (*21a*); [b] Q-dependence of the scattering over the range $0.006 \leq Q \leq 0.08$ Å^{-1}; [c] Equations SI-3 & SI-10 in (*21b*); [d] Equation SI-11a in (*21b*); [e] Equations SI-4a & SI-4b in the present Supporting Information.

Table 2. Structural characteristics for the peroxide-treated sediment samples and replicates 'off-match' before and after addition of PHA and in the presence of background electrolyte. For comparison, Sample 'E1.1' is reproduced from Table 1. Dimensions are rounded to the nearest nm, aggregation numbers to the nearest whole number. Indicative errors on the fractal dimensions represent one standard deviation as derived from the model-fitting analysis.

Code	Sample & Matrix	ϕ [a]	n [b]	Fractal Aggregates Model [c]				
		%		R_{pri} (nm)	N_{agg}	τ	D_m	ψ (nm)
	In H_2O:							
E1.1	Native wet sediment (Replicate #1)	1.90	3.30	3	11	1.30	2.47 ± 0.02	8
E1.7	Short-term peroxide-treated wet sediment (Replicate #1)	1.06	3.27	15	3	1.33	2.08 ± 0.07	22
E1.8	Short-term peroxide-treated wet sediment (Replicate #2)	1.16	3.31	34	2	1.46	2.19 ± 0.01	42
E1.11	Long-term peroxide-treated wet sediment	1.89	3.31	4	7	1.36	2.61 ± 0.01	8
E3.1	Short-term peroxide-treated wet sediment + 255 mg/L PHA, pH6	1.20	3.30	18	5	1.31	2.01 ± 0.07	31
E3.2	Short-term peroxide-treated wet sediment + 380 mg/L PHA, pH6	1.27	3.27	8	5	1.35	2.25 ± 0.07	13
	In 2mM $CaCl_2$ / H_2O:							
E3.3	Short-term peroxide-treated wet sediment + 255 mg/L PHA, pH6	1.39	3.29	8	5	1.34	2.26 ± 0.01	14
E3.4	Short-term peroxide-treated wet sediment + 380 mg/L PHA, pH6	1.47	3.21	3	9	1.34	2.60 ± 0.01	8
	In D_2O:							
E3.6	Short-term peroxide-treated wet sediment + 380 mg/L PHA, pH6	1.48	3.23	2	15	1.35	2.69 ± 0.01	6

[a] Assuming a mineral density of 2.75 g/cm^3 (*21a*); [b] Q-dependence of the scattering over the range $0.006 \leq Q \leq 0.08$ Å^{-1}; [c] Equations SI-4a & SI-4b in the present Supporting Information.

Table 3. Structural characteristics for the peroxide-treated sediment samples and replicates at contrast match before and after addition of PHA and in the presence of background electrolyte. For comparison, Sample 'E1.1' is reproduced from Table 1 and Samples 'E3.1' & 'E3.2' are reproduced from Table 2. Dimensions are rounded to the nearest nm, aggregation numbers to the nearest whole number. Indicative errors on the fractal dimensions represent one standard deviation as derived from the model-fitting analysis.

Code	Sample & Matrix	ϕ [a]	n [b]	Fractal Aggregates Model [c]				
		%		R_{pri} (nm)	N_{agg}	τ	D_m	ψ (nm)
	In H_2O:							
E1.1	Native wet sediment (Replicate #1)	1.90	3.30	3	11	1.30	2.47 ± 0.02	8
E3.1	Short-term peroxide-treated wet sediment + 255 mg/L PHA, pH6	1.20	3.30	18	5	1.31	2.01 ± 0.07	31
E3.2	Short-term peroxide-treated wet sediment + 380 mg/L PHA, pH6	1.27	3.27	8	5	1.35	2.25 ± 0.07	13
	In Contrast Match H_2O / D_2O:							
E2.11	Native wet sediment	1.70	2.81	1	6	1.50	2.66 ± 0.01	3
E2.14	Short-term peroxide-treated wet sediment	1.62	3.26	3	9	1.32	2.71 ± 0.01	7
E3.7	Short-term peroxide-treated wet sediment + 255 mg/L PHA, pH6	1.20	3.37	57	6	1.30	1.94 ± 0.01	112
E3.8	Short-term peroxide-treated wet sediment + 380 mg/L PHA, pH6	1.43	3.33	4	11	1.32	2.47 ± 0.02	10
	In 2mM $CaCl_2$ in Contrast Match H_2O / D_2O:							
E2.12	Native wet sediment	1.77	2.81	2	6	1.48	2.58 ± 0.02	4

[a] Assuming a mineral density of 2.75 g/cm^3 (*21a*); [b] Q-dependence of the scattering over the range $0.006 \leq Q \leq 0.08$ Å^{-1}; [c] Equations SI-4a & SI-4b in the present Supporting Information.